0.5 wt% Ru/γ-Al_2O_3 is a highly active and stable catalyst for direct conversion of biogas into renewable natural gas

Yichen Zhuang, David S. A. Simakov*

Department of Chemical Engineering, University of Waterloo, Waterloo ON N2L 3G1, Canada

ABSTRACT

Landfill gas is a source of CH_4 emission, also rich in CO_2 (up to 50 vol%). It can be upgraded to renewable natural gas (RNG) by separating CO_2 and impurities. Alternatively, the CO_2 contained in biogas can be converted into CH_4 via the Sabatier reaction, using H_2 generated by water electrolysis. For industrial applications, it is beneficial to eliminate the energy intensive CO_2 separation step, converting biogas to RNG directly. In this work, a series of 0.02-1 wt% Ru/γ-Al_2O_3 catalysts were prepared by wet impregnation and evaluated for a single-pass conversion of CO_2-CH_4 mixtures. Through the catalytic performance evaluation and characterization studies, the optimal Ru loading was identified as 0.1-0.5 wt%. For these catalysts, CO_2 conversion of 80-87% was achieved at 450 °C and 90,000 mL/(g h), maintaining 95-99% selectivity to CH_4 production. These catalysts also showed excellent stability over 100 h on stream, while maintaining 99-100% CH_4 selectivity.

Keywords: Landfill gas; CO_2 methanation; Renewable natural gas; Ru/γ-Al_2O_3.

* *Corresponding author.* Tel.: +1 519 8884567; E-mail addresses: dsimakov@uwaterloo.ca

1. Introduction

Biogas (including landfill gas) is a renewable feedstock produced in the anaerobic fermentation process. Biogas typically consists of 50-70% CH_4 and 25-45% CO_2, with relatively small quantities of N_2 and H_2O, as well as trace amounts of O_2, hydrogen sulfide (H_2S) and volatile organic compounds (VOCs) [1, 2]. The use of biogas and landfill gas as a substitute feedstock to fossil natural gas (NG) has a potential to reduce CO_2 emissions significantly [3]. Such substitute natural gas obtained from non-fossil feedstocks is typically referred to as renewable natural gas (RNG) [3]. It is important to note that the CO_2, which is eventually emitted as a result of utilization of RNG (combustion), is of biological origin thus does not add carbon to the atmosphere. At the same time the use of RNG results in CO_2 emission reduction due to the fossil NG displacement and incorporation of renewable electricity into the energy sector.

Despite abovementioned advantages, utilization of biogas and landfill gas as alternative feedstocks has a number of technological challenges. First, the CH_4 content is not as high as in the industrial grade NG, thus these streams need to be upgraded prior to use. Second, biogas contains trace amounts of contaminants and VOCs with some of them being hazardous to the environment and processing equipment. Extra purification procedures are required to improve the quality of the gas. Current, commercially available technologies for processing biogas and landfill gas are based on concentrating CH_4 via CO_2 separation and removal of impurities such as water vapor, H_2S and siloxanes [4]. Landfill gas in particular contains non-negligible quantities of O_2 and N_2, which have to be separated prior to the use as well. CO_2 separation, which is the most energy intensive stage, can be done by pressure swing adsorption (PSA) on molecular sieves or activated carbon, membrane separation, as well as by cryogenic methods [5, 6]. High operation costs and large

capital investment associated with the abovementioned technologies limit the economic viability of the biogas and landfill gas utilization on an industrial scale.

An alternative way is the thermocatalytic conversion of CO_2 into synthetic fuels via reverse water gas shift (RWGS) and methanation reactions, Eqs (1-3) [3]:

$$CO_2 + H_2 \rightleftarrows CO + H_2O \qquad \Delta H^{\circ}_{298} = 41 \text{ kJ/mol} \tag{1}$$

$$CO_2 + 4H_2 \rightleftarrows CH_4 + 2H_2O \qquad \Delta H^{\circ}_{298} = -164.9 \text{ kJ/mol} \tag{2}$$

$$CO + 3H_2 \rightleftarrows CH_4 + H_2O \qquad \Delta H^{\circ}_{298} = -206.1 \text{ kJ/mol} \tag{3}$$

The RWGS reaction can be used to produce syngas which can be later utilized to produce methanol or higher hydrocarbons via the Fischer-Tropsch process [3]. However, for biogas and landfill gas this approach can be only valid if CO_2 is separated first. CO_2 methanation via the Sabatier reaction, Eq. (2), is a better choice, especially if it can be done directly, eliminating CO_2 separation costs. The process of landfill gas and/or biogas direct upgrading is conceptually shown in Fig. 1. H_2 required for CO_2 methanation can be obtained from water electrolysis powered by renewable or (low carbon footprint) surplus electricity. After the purification step to remove impurities such as H_2S, VOCs and siloxanes, the CO_2/CH_4 mixture is fed to the Sabatier reactor, e.g., packed bed [7, 8]. A pipeline grade RNG is obtained from the reactor outlet after water condensation and further product upgrading (removal of N_2 and unreacted CO_2 and H_2), if required. Electrolysis, as well as all purification, condensation and upgrading stages are commercially available and the economic viability of the concept presented in Fig. 1 was recently assessed, leading to positive conclusions [9]. However, reactor design [7, 8] and catalysis still present significant technological challenges.

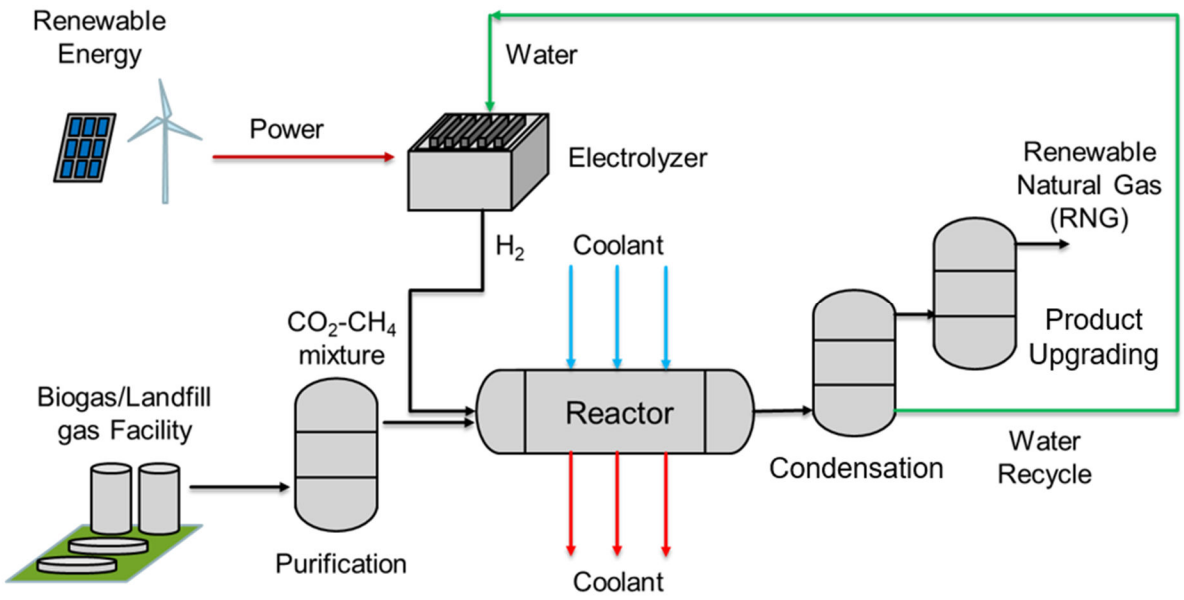

Fig. 1. A conceptual diagram of the direct upgrade of biogas or landfill gas into renewable natural gas (RNG).

Over the years many catalytic formulations have been suggested for CO_2 methanation, including supported noble metals and Ni-based formulations. Ni catalysts are usually supported on high surface area alumina [10], typically exhibiting good performance. For example, CO_2 conversion of 81% and CH_4 selectivity of 96% were achieved using a 20 wt% Ni/Al_2O_3 catalyst at 400 °C and space velocity of 55,000 h^{-1} [11]. It has been also found that addition of Yb_2O_3 can significantly improve the stability of Ni/Al_2O_3 catalysts (long-term stability is one of the major concerns in the use of Ni-based catalysts) [12]. Using Y_2O_3 as a sole support was also demonstrated, obtaining 76% CO_2 conversion and 100% CH_4 selectivity at 300 °C and H_2:CO_2 = 4 over the Ni/Y_2O_3 catalyst [13]. Other supports such as SiO_2 and MgO were also studied showing generally good performance over short operation periods [14, 15].

One of the main drawbacks of Ni-based catalysts is (undesired) CO formation, which can be significant under certain conditions; CO was confirmed as a reaction intermediate for Ni-catalyzed methanation reaction [13]. Another disadvantage is poor stability over extended periods of operation, which is attributable to sintering and coking [16]. Noble metals such as Ru, Ir, Rh, Os, Pt and Pd generally have high catalytic activity and excellent resistance against coking [17]; Ru is known as a good CO_2 methanation catalyst. CO_2 conversion of 55% and CH_4 selectivity of 95% were achieved over the 5 wt% Ru/Al_2O_3 catalyst at 350 °C and $H_2:CO_2 = 3$ [18]. In another study, 93% CO_2 conversion and complete selectivity to CH_4 were reported over the 3 wt% Ru/Al_2O_3 catalyst at 325 °C and GHSV = 55,000 h^{-1} [11]. The main drawback in the use of noble metals is the high material cost, thus minimizing the active phase loading is of paramount importance [19].

In this paper, we investigated the catalytic performance of $Ru/\gamma\text{-}Al_2O_3$ in direct conversion of CO_2/CH_4 mixtures, simulating the biogas and landfill gas composition. Ru was selected as the least expensive among the platinum group metals [19]. Ru content ranging from 0.02-1wt% were prepared and tested to identify the lowest possible Ru loading. Catalytic performance was evaluated in terms of CO_2 conversion and selectivity to CH_4 over the range of temperatures, space velocities, pressures and H_2/CO_2 ratio. CO_2 conversion of up to 80-87% with nearly complete selectivity to CH_4 production was achieved at 450 °C for Ru loadings of 0.1-1wt%. For lower Ru loadings (0.02-0.05 wt%), both CO_2 conversion and CH_4 selectivity dropped very significantly. No decline in conversion or selectivity was detected for the 0.5wt% $Ru/\gamma\text{-}Al_2O_3$ catalyst over 115 h on stream. To the best of our knowledge, we report the first study of direct conversion of CO_2/CH_4 mixtures, showing very promising results in terms of conversion, selectivity and stability.

2. Experimental

2.1 Catalyst preparation and characterization

A series of Ru/γ-Al_2O_3 catalysts with Ru loading ranging from 0.02-1 wt% were prepared using a sonication-assisted, wet impregnation method that allows for excellent Ru dispersion [19]. Commercial alumina support pellets (γ-Al_2O_3, 250 m^2/g, Alfa Aesar) were crushed and sieved to 250-425 μm particles prior to impregnation. Appropriate amounts of ruthenium chloride ($RuCl_3 \times H_2O$, 37.5wt% Ru, Alfa Aesar) were dissolved in acetone (99.5%, Fisher Scientific) and the sieved γ-Al_2O_3 particles were added to the solutions with different Ru concentrations. The resulted slurries were sonicated for 30 min in 20 mL vials placed in an ultrasonic bath (Fisher Scientific). After sonication, the slurries were dried in air at 60 °C.

Inductively coupled plasma mass spectrometry (ICP-MS, Prodigy SPEC, Leeman Labs Inc.) was used to confirm Ru loadings. A surface area analyzer (Gemini VII 2390, Micromeritics Instrument Corporation) was used to measure the specific surface area (SSA) using N_2 as adsorption gas. Temperature programmed oxidation (TPO) of spent catalysts was conducted to determine the extent of coking. The air flow rate of TGA (TGA55, TA Instruments) was 40 ml/min and temperature ramping rate was set to 10 °C/min for T ≤ 150 °C and 2 °C/min for T = 150-700 °C. The exhaust gas from TGA was measured by an inline FTIR analyzer (MultiGas™ 2030, MKS Instruments). Pulse chemisorption and temperature programmed reduction (TPR) measurements were both conducted using the AMI300 catalyst characterization system (AMI300 Lite, Altamira Instruments). For pulse chemisorption, the samples were pretreated in 10% H_2/Ar for 1 h at 350 °C and then cooled down to ambient temperature to start pulse chemisorption. 10% H_2/Ar and Ar were used as pulse gas and carrier gas respectively. For TPR, the samples were

pretreated under Ar at 150 °C to remove moisture, cooled down to 100 °C and then heated up to 700 °C at the rate of 2 °C/min in 10% H_2/Ar.

2.2 Catalytic performance evaluation

The flow system setup for conducting reaction tests is shown in Fig. 2. The reactor, made from a stainless steel 1/4″ Swagelok tee connected on both sides to 1/4″ stainless steel tubing (Swagelok), was placed in a furnace (Lindberg/Blue M™ Mini-Mite™ Tube Furnaces, Thermo Fisher Scientific). The remaining tee connector opening was used to load the catalyst (~ 200 mg) and was sealed with a stainless-steel plug (Swagelok). Temperature was controlled by a build-in temperature controller (UP150, Yokogawa). A K-type thermocouple (1/8″, Omega Engineering) was placed inside the reactor in contact with the catalyst. Feed flow rates were controlled with mass flow controllers (EL-FLOW Series, Bronkhorst High-Tech). Pressure was adjusted by a back pressure regulator (S01094789B, Swagelok). In the product stream, water was removed by a mist trap (AFM40-N02-Z-A, SMC Corporation) and a moisture trap (5182-9411, Agilent Technologies; the original moisture adsorbent was replaced with orange silica gel, Fisher Scientific). Outlet concentrations were measured on dry basis (after removal of condensed water and humidity) using the IR analyzer (IR-208, Infrared Industries, Inc., USA) continuously monitored with LabVIEW (National Instruments) using an analog-to-digital converter (USB 6008, National Instruments).

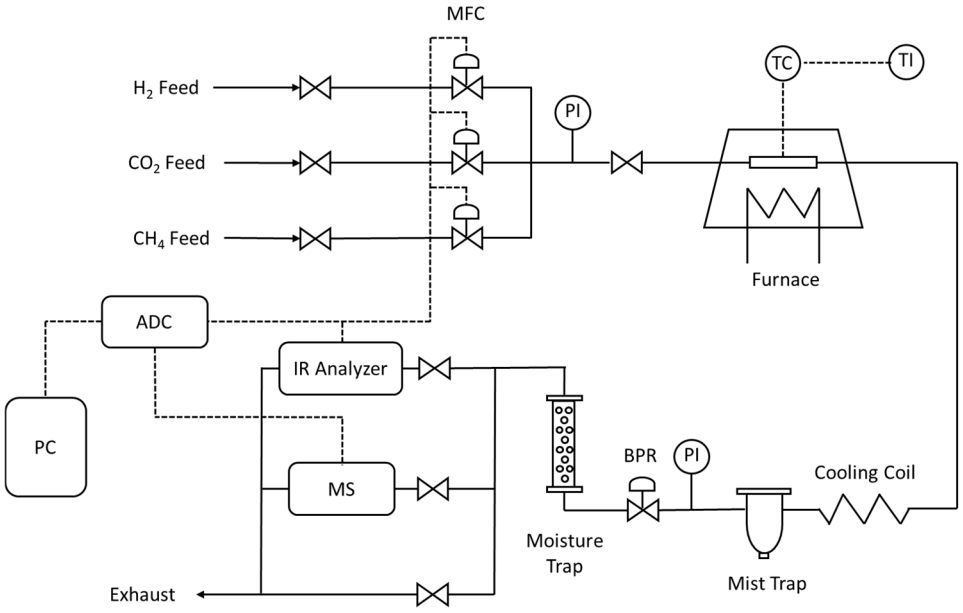

Fig. 2. Flow system setup for conducting catalytic performance evaluation.

Catalytic performance was evaluated in the 350-600 °C temperature range and 90,000-420,000 mL/(g h) gas hourly space velocity (GHSV) range. Pressure of 3 bar and feed ratios of H_2:CO_2 = 4 and CH_4:CO_2 = 1 were kept in all experiments, except for one stability test with a simulated landfill gas composition. This test was conducted with the 30% CO_2, 43% CH_4 and 27% N_2 mixture (H_2/CO_2 = 4) in the 1-9 bar pressure range.

CO_2 conversion (X_{CO_2}) and CH_4 selectivity (S_{CH_4}) were obtained from the following equations (y_{CO_2}, y_{CO}, and y_{CH_4} are mole fractions measured by the IR analyzer on dry basis):

$$X_{CO_2} = \frac{y_{CO} + y_{CH_4} - \beta(y_{CO} + y_{CO_2} + y_{CH_4})}{(1-\beta)(y_{CO} + y_{CO_2} + y_{CH_4})} \tag{4}$$

$$S_{CH_4} = \frac{y_{CH_4} - \beta(y_{CO} + y_{CO_2} + y_{CH_4})}{y_{CO} + y_{CH_4} - \beta(y_{CO} + y_{CO_2} + y_{CH_4})} \tag{5}$$

To obtain Eqs (4, 5), CO_2 conversions to CO, Eq. (6), and to CH_4, Eq. (7), are first defined ($F_{CO_2,f}$ and $F_{CH_4,f}$ are the feed molar flow rates of CO_2 and CH_4, $F_{CO,out}$ is the outlet CO molar flow rate, and $F_{CH_4,gen}$ is the molar flow rate of generated CH_4):

$$f_1 = \frac{y_{CO}}{(1-\beta)(y_{CO} + y_{CO_2} + y_{CH_4})} \equiv \frac{F_{CO,out}}{F_{CO_2,f}} \tag{6}$$

$$f_2 = \frac{y_{CH_4} - \beta(y_{CO} + y_{CO_2} + y_{CH_4})}{(1-\beta)(y_{CO} + y_{CO_2} + y_{CH_4})} \equiv \frac{F_{CH_4,gen}}{F_{CO_2,f}} \tag{7}$$

β is the CH_4 content in the feed, as defined by Eq. (8):

$$\beta = \frac{F_{CH_4,f}}{F_{CH_4,f} + F_{CO_2,f}} \equiv \frac{F_{CH_4,f}}{F_{C,f}} \tag{8}$$

The total CO_2 conversion and CH_4 selectivity are then obtained as follows:

$$X_{CO_2} = f_1 + f_2 \tag{4a}$$

$$S_{CH_4} = \frac{f_2}{f_1 + f_2} \tag{5a}$$

Carbon balance (*CB*) is defined as the total rate of carbon fed to the reactor divided by the rate of carbon exiting the reactor:

$$CB = (y_{CO_2} + y_{CO} + y_{CH_4})(1 + \alpha - f_1 - 4f_2 + \gamma)(1-\beta) \tag{9}$$

In Eq. (9), the feed H_2:CO_2 ratio (α) and feed CH_4:CO_2 ratio (γ) are defined as follows ($F_{H_2,f}$ is the feed H_2 flow rate):

$$\alpha = \frac{F_{H_2,f}}{F_{CO_2,f}} \tag{9a}$$

$$\gamma = \frac{F_{CH_4,f}}{F_{CO_2,f}} \tag{9b}$$

To obtain Eq. (9), the carbon balance definition, Eq. (9c), is expressed in terms of α, β, γ, f_1 and f_2 using the total outlet flow rate $F_{t,out}$ defined by Eq. (9d):

$$CB = \frac{F_{C,out}}{F_{C,f}} = \frac{(y_{CO_2} + y_{CO} + y_{CH_4})F_{t,out}}{F_{CO_2,f}/(1-\beta)} \tag{9c}$$

$$F_{t,out} = F_{CO_2,f} + [F_{H_2,f} - F_{CO,out} - 4(F_{CH_4,out} - F_{CH_4,f})] + F_{CH_4,f} \tag{9d}$$

$F_{CO,out}$ and $F_{CH_4,out}$ in Eq. (9d) correspond to the H_2 consumption in the RWGS and Sabatier reactions, Eqs (1, 2). In all testes conducted carbon balance was monitored and recorded continuously with LabVIEW. Deviations of carbon balance did not exceed 5%, i.e., the carbon balance was in the CB = 0.95-1.05 range.

CH_4 generation rate per catalyst weight (r) and per active phase weight (R) was calculated by Eqs (10, 11) (W_c is catalyst weight and L_{Ru} is Ru loading in %):

$$r_{CH_4} = \frac{F_{CO_2,f} X_{CO_2} S_{CH_4}}{W_c} \tag{10}$$

$$R_{CH_4} = 100\frac{r_{CH_4}}{L_{Ru}} \tag{11}$$

Turnover frequency was calculated from Eq. 12 (M_{Ru} is atomic weight and D is the metal dispersion obtained by chemisorption, as calculated by Eq. 13):

$$TOF = \frac{M_{Ru} \times R_{CH_4}}{D} \tag{12}$$

$$D = \frac{100 \times HU \times M_{Ru} \times 2}{L_{Ru}} \tag{13}$$

HU in Eq. (13) is the chemisorption H_2 uptake in mole per gram catalyst and 2 is the stoichiometric factor for H_2 chemisorption. The corresponding particle size (in nm) is calculated by the following equation:

$$d_p = \frac{6 \times 10^9 \times M_{Ru} \times \rho_{site}}{\rho_{Ru} \times N_A \times D} = \frac{1.32}{D} \tag{14}$$

The site density (ρ_{site}) is 16.3 Ru atoms per nm^2 [20] (used in $1/m^2$ in Eq. (14) for units consistency), which is equivalent to the 0.061 nm^2 site area.

3. Results and discussion

3.1 Catalyst characterization

Ru loadings in freshly prepared catalysts were confirmed using ICP-OES. Note that the preparation procedure did not include any washing, only evaporation (see Section 2.1), which allows for a precise active phase loading. The BET surface area of freshly prepared samples was measured as 210±5 m^2/g, as compared to 206 m^2/g measured for the γ-Al_2O_3 support before Ru impregnation. Some reduction of the specific surface area as compared to the 250 m^2/g specified by the supplier (Alfa Aesar) cab be related to crashing and sieving procedure (see Section 2.1). As expected, the simple Ru impregnation routine did not affect significantly the specific surface area. Representative TEM images of the 0.5 wt% Ru/γ-Al_2O_3 catalyst after the reaction test are shown in Fig. 3, where 2-3 nm Ru nanoparticles well-dispersed on fiber-like γ-Al_2O_3 grains can be seen. Ru nanoparticles appear as dark spots, due to their higher electron density. Fiber-like shape is a

typical morphology of γ-Al_2O_3 [21]. The obtained morphology was typical of Ru/γ-Al_2O_3 catalysts prepared by the sonication-assisted wet impregnation procedure [19].

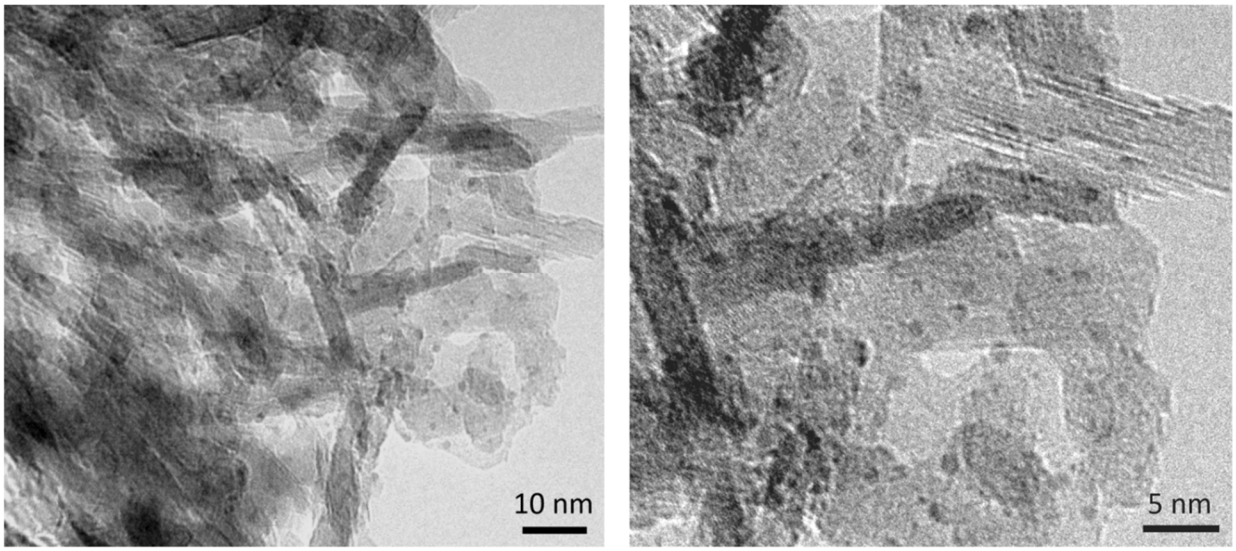

Fig. 3. TEM micrographs of the 0.5 wt% Ru/γ-Al_2O_3 catalyst after reaction test.

Temperature programmed reduction (TPR) profiles of the 0.02, 0.5 and 1 wt% Ru/γ-Al_2O_3 as prepared catalysts are shown in Fig. 4. For the 0.5 wt% and 1 wt% Ru catalyst profiles are qualitatively similar. The three observed peaks are located at around 150 °C, 350 °C and 530 °C. Low temperature TPR peaks for supported Ru catalysts are typically attributed to well-dispersed RuO_x species [22], while higher temperature peaks are normally associated with either bulk RuO_2 or Ru strongly bonded on a support [23-25].

Generally speaking, under a linear heating TPR profile the reduction temperature of a supported metal catalyst is affected by both the metal oxide particle size and the metal-support interaction magnitude. For a smaller particle size, the reduction peak will appear at a lower temperature. On the other hand, strong particle-support interaction will shift the reduction peak to a higher temperature. Since the particle size appears to be relatively small, as evident from the

TEM analysis (see Fig. 3 and elsewhere [19]), the (unusually) high temperature reduction peaks can be attributed to the strong metal-support interaction. The appearance of three different peaks indicates the existence of RuO_x species with different oxidation states and particle size. As it was previously reported for Ru/γ-Al_2O_3 prepared by the same procedure, for increasing Ru loadings the Ru particle size distribution becomes bimodal [19]. The TPR profile of the 0.02 wt% Ru catalyst showed a completely different shape, with a reduction peak centered at 400 °C. The appearance of a single peak may indicate the existence of a much narrower particle size distribution, with the Ru nanoparticles strongly interacting with the γ-Al_2O_3 support.

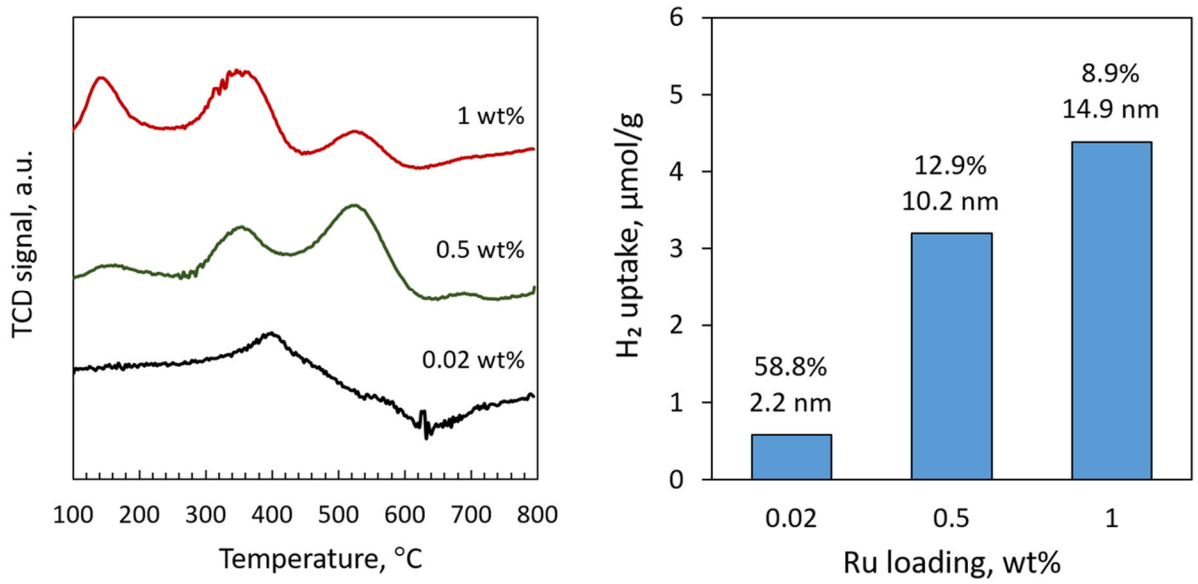

Fig. 4. The effect of Ru loading on the temperature-programmed reduction (TPR) profiles (left panel) and H_2 chemisorption (right panel), showing also the measured dispersion values with corresponding calculated crystallite size.

The H_2 pulse chemisorption results are shown on the right panel of Fig. 4, alongside with corresponding values of dispersion and particle diameter as calculated by Eqs (13, 14). While the

H_2 uptake increases with increased Ru loading, the metal dispersion decreases and the corresponding particle size decreases. These trends are expected, as for increasing Ru loading particle size distribution becomes broader, with a significant population of larger particles [19]. The particle size calculated for the 0.5 wt% Ru catalyst is significantly higher (approximately 3-fold) than that expected from the TEM analysis (Fig. 3). However, Eq. (14) does not account for polydispersity. Also, some of the Ru nanoparticles may not be fully exposed to the gas phase during the chemisorption experiment that will lead to a lower measured dispersion and, as a result a larger calculated particle size. Nevertheless, the H_2 chemisorption results indicate the increased degree of metal dispersion for decreased Ru loading, which is expected and consistent with other previous reports [18].

In the next two sections, the catalytic performance of a selected Ru loading (0.5 wt%) is first examined and the effect of Ru loading is then investigated. It is important to emphasize at this point that the results reported are on CO_2 conversion in a CO_2/CH_4 mixture, not pure CO_2 conversion. After the investigation of the effect of Ru loading, stability tests are reported in Section 3.4, on CO_2 conversion in CO_2/CH_4 and $CO_2/CH_4/N_2$ mixtures, simulating realistic landfill gas composition (after removal of impurities).

3.2 Catalytic performance evaluation

The catalytic performance of the 0.5 wt% Ru/γ-Al_2O_3 catalyst as a function of temperature and space velocity is shown in Fig. 5. Error bars show standard deviation between three separate measurements obtained with different catalyst batches; good repeatability between different data sets were obtained. Equilibrium curves (shown as solid lines) were calculated as explained in the Appendix. Note that the equilibrium conversion of the 50:50 CO_2/CH_4 mixture is 96% at 300 °C and the selectivity to CH_4 formation is nearly 100% below 450 °C. This outcome is important

because CH_4 can potentially react with H_2O (the product of the methanation reactions and RWGS) via steam reforming producing CO. Therefore, it is expected that operating at low space velocities (large residence times) and as low as possible temperatures will be necessary.

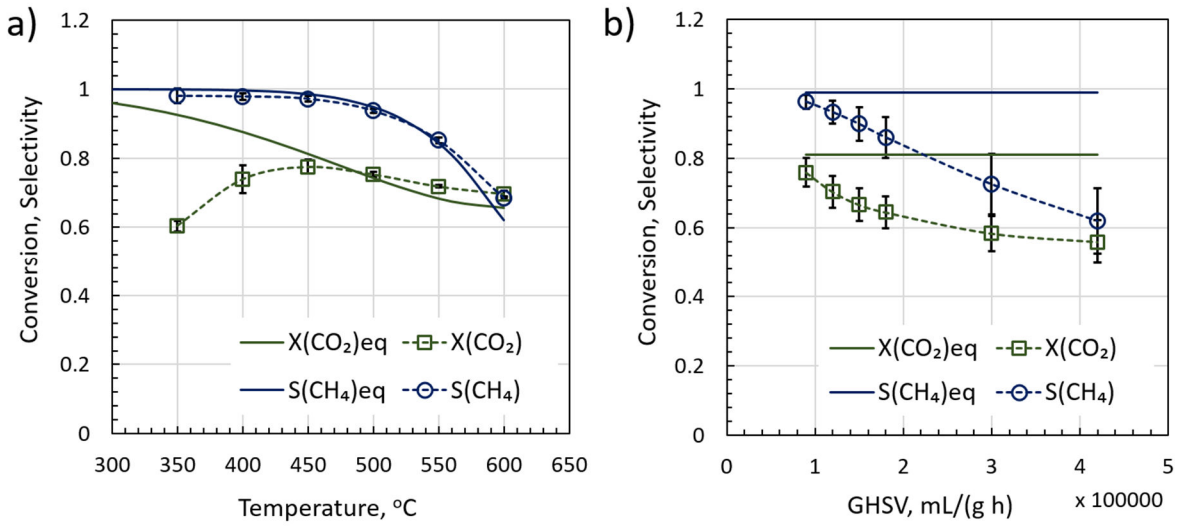

Fig. 5. Catalytic performance of 0.5 wt% Ru/γ-Al_2O_3 in terms of CO_2 conversion, $X(CO_2)$, and CH_4 selectivity $S(CH_4)$ as a function of temperature (a) and space velocity (b). Solid lines show equilibrium values. Error bars show standard deviation of 3 separate experiments. *Parameters:* H_2:CO_2 = 4, CH_4:CO_2 = 1, P = 3 bar, GHSV = 90,000 mL/(g h) (a), T = 450 °C (b).

At GHSV = 90,000 mL/(g h) CH_4 selectivity is nearly 100% in the 350-450 °C range and decreasing gradually for higher temperatures following the equilibrium curve (Fig. 5a). CO_2 conversion increases from 60% at 350 °C to nearly 80% at 450 °C, where it achieves the equilibrium value and then follows the equilibrium curve for higher temperatures (Fig. 5a). The decline in CH_4 selectivity (predicted by thermodynamic equilibrium) is in line with the fact that the RWGS and methanation reactions are endothermic and exothermic, respectively, Eqs (1-3). As a result, CO generation is expected to be more significant at higher temperatures. Another possible

pathway for CO formation could be CH_4 steam reforming, the reverse, endothermic reaction in Eq. (3). The deviation of the experimentally measured CO_2 conversion from the equilibrium curve for T < 450 °C (Fig. 5a) is due to kinetic limitations, which can be clearly observed in Fig. 5b.

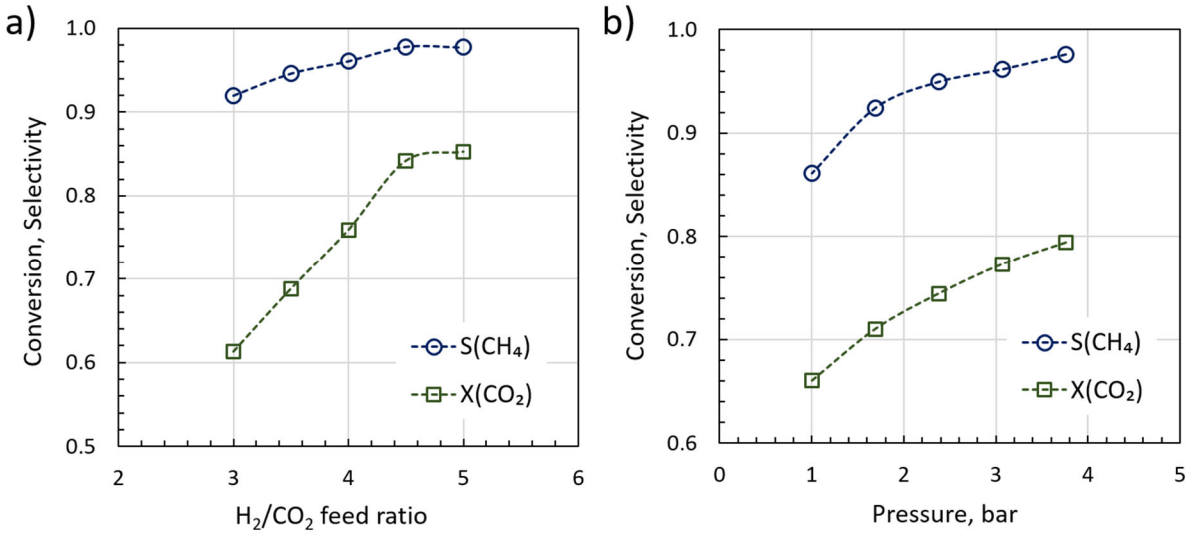

Fig. 6. Catalytic performance of the 0.5wt% Ru/γ-Al_2O_3 catalyst as a function of the feed H_2:CO_2 ratio (a) and operating pressure (b). *Parameters:* T = 450 °C, GHSV = 90,000 mL/(g h), CH_4:CO_2 = 1, P = 3 bar (a), H_2:CO_2 = 4 (b).

For increasing space velocities (shorter residence time) CO_2 conversion at 450 °C departs from its equilibrium value and declines gradually. Interestingly, CH_4 selectivity decreases very significantly as well. This decline could be attributes to different reaction rate scales of RWGS and methanation, i.e., if the RWGS rate is much faster than those for methanation reactions, it will be less affected by shorter contact times, resulting in a higher selectivity to CO formation. From a practical point of view, space velocities should be kept below 100,000 mL/(g h) in order to keep high CH_4 selectivity. Note that GHSV = 100,000 mL/(g h) corresponds to a residence time of ca. 10 ms ($1/\tau = GHSV \times \rho_b/\varepsilon$; τ is residence time, ρ_b and ε are bulk catalyst density and catalyst bed

void fraction; ρ_b/ε = 4 g/mL), thus even operating at GHSV = 1,000 mL/(g h) will be industrially relevant (residence time on a scale of seconds).

The effects of the feed H_2:CO_2 ratio and operating pressure are shown in Fig. 6 at selected temperature and GHSV of 450 °C and 90,000 mL/(g h). Increasing the feed H_2:CO_2 ratio from 3 to 5 results in a very significant conversion gain, from 60% to 85%. The selectivity to CH_4 generation increases from 92% to 97%. Clearly, the feed H_2:CO_2 ratio is an important operation parameter. However, from a practical point of view there is a tradeoff between the positive effect on CH_4 yield and additional capital and operating costs required for separating unreacted H_2 from a product stream. The effect of operating pressure on CH_4 yield is also positive, Fig. 6b. A minor increase in (absolute) pressure from 1 bar to 3.8 bar results in a very significant gain in both conversion and selectivity, reaching 80% CO_2 conversion and 98% CH_4 selectivity at 3.8 bar and H_2:CO_2 = 4 in the feed. For practical purposes moderate pressure increase can be very beneficial because, in addition to improved CH_4 yield, it will lead to more compact equipment with a relatively low operating cost increase for compression. In general, the trends observed in Fig. 6 are expected from the thermodynamic point of view, as both pressure and excess H_2 favor methanation reactions that result in a decrease in total number of moles, Eqs (2, 3).

3.3 The effect of Ru loading

To identify the lowest possible Ru loading, a series of catalysts with Ru loading ranging from 0.05-1 wt% were tested. Catalytic performance was evaluated in a range of temperatures (Fig. 7) and space velocities (Fig. 8). As expected, decreasing the active phase loading for the given space velocity shifts the conversion curve away from the equilibrium line, with a more pronounced effect at lower temperatures, Fig. 7. This decrease can be attributed to kinetic limitations, i.e. lower

number of active sites for lower loading (assuming comparable active phase dispersion). At 90,000 mL/(g h) in the 450-600 °C range, an order of magnitude decrease in Ru loading from 1 wt% to 0.1 wt% results in only a minor loss in conversion.

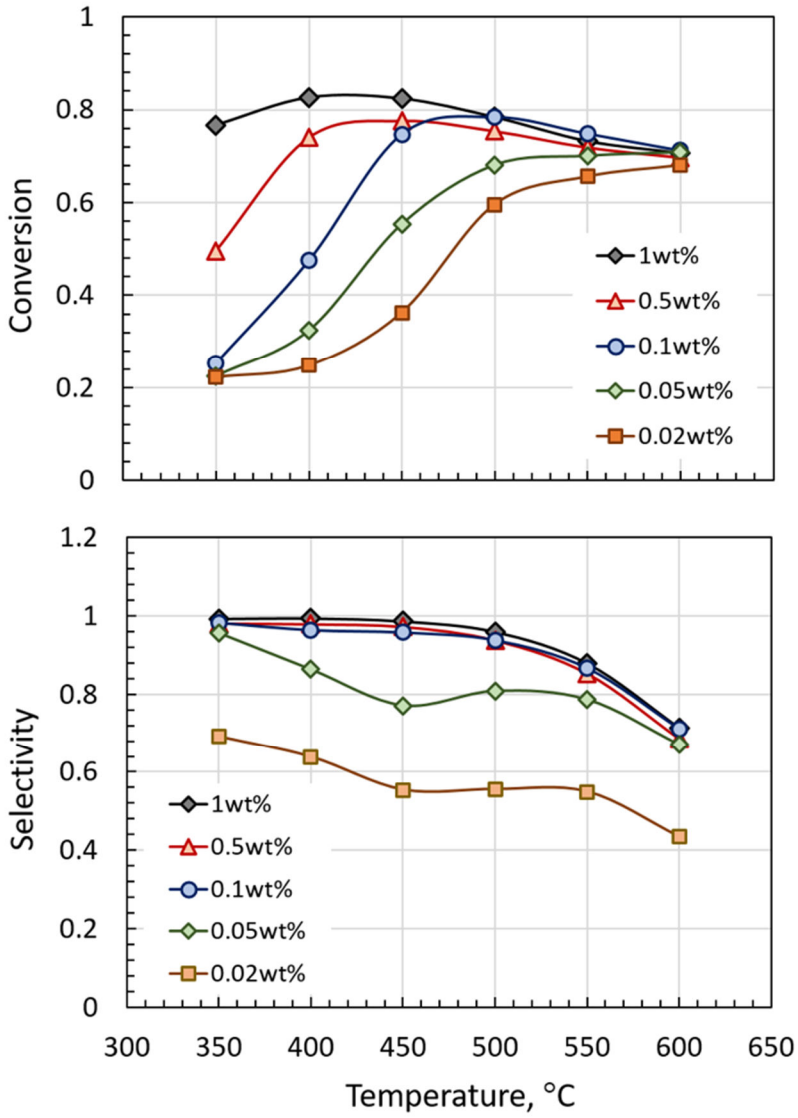

Fig. 7. CO_2 conversion and CH_4 selectivity of 0.02-1wt% Ru/γ-Al_2O_3 catalysts as a function of temperature. *Parameters*: GHSV = 90,000 mL/(g h), H_2:CO_2 = 4, CH_4:CO_2 = 1, P = 3 bar.

The selectivity to CH_4 generation follows the equilibrium curve for 0.1-1 wt% Ru. Thus, for the set of operating conditions given in Fig. 7, operating in the 450-500 °C can allow a 10-fold decrease in the active phase loading. However, conducting a highly exothermic Sabatier reactor in this temperature regime can be challenging, which points out at a paramount importance of thermal managing (proper reactor cooling) [7, 8]. Lowering the Ru loading below 0.1 wt% (0.05 and 0.02 wt%) leads to a very significant drop in selectivity, in particular for 0.02 wt% Ru, Fig. 7. This finding is in line with another study reported in the literature, showing a clear correlation between decreasing Ru loadings and increasing CO yields (ca. 10-20%) at 400-500 °C, although in a different Ru loading range (5-0.1 wt%) and using a different catalyst preparation procedure [18].

Examining the performance of the 0.05-1 wt% catalysts as a function of space velocity shows similar trends, Fig. 8. The (expected) decline in conversion and selectivity vs. space velocity for 0.1-1 wt% is significant but not drastic. This trend is in line with the one presented in Fig. 5 (see corresponding discussion). On the other hand, the 0.02 wt% and 0.05 wt% catalysts lose the CO_2 conversion more rapidly for increasing space velocities. The observed fast decline indicates that the 0.02 wt% and 0.05 wt% catalysts are significantly less active, which is in line with the trend observed in Fig, 7. The decrease in selectivity vs. space velocity is also more pronounced for the 0.02 wt% and 0.05 wt% catalysts as compared to the 0.05-1 wt% Ru loadings. As was previously discussed (see Fig. 5 and corresponding discussion), the declining CH_4 selectivity for shorter residence times can be attributed to the different reaction rate scales of the RWGS and methanation reactions.

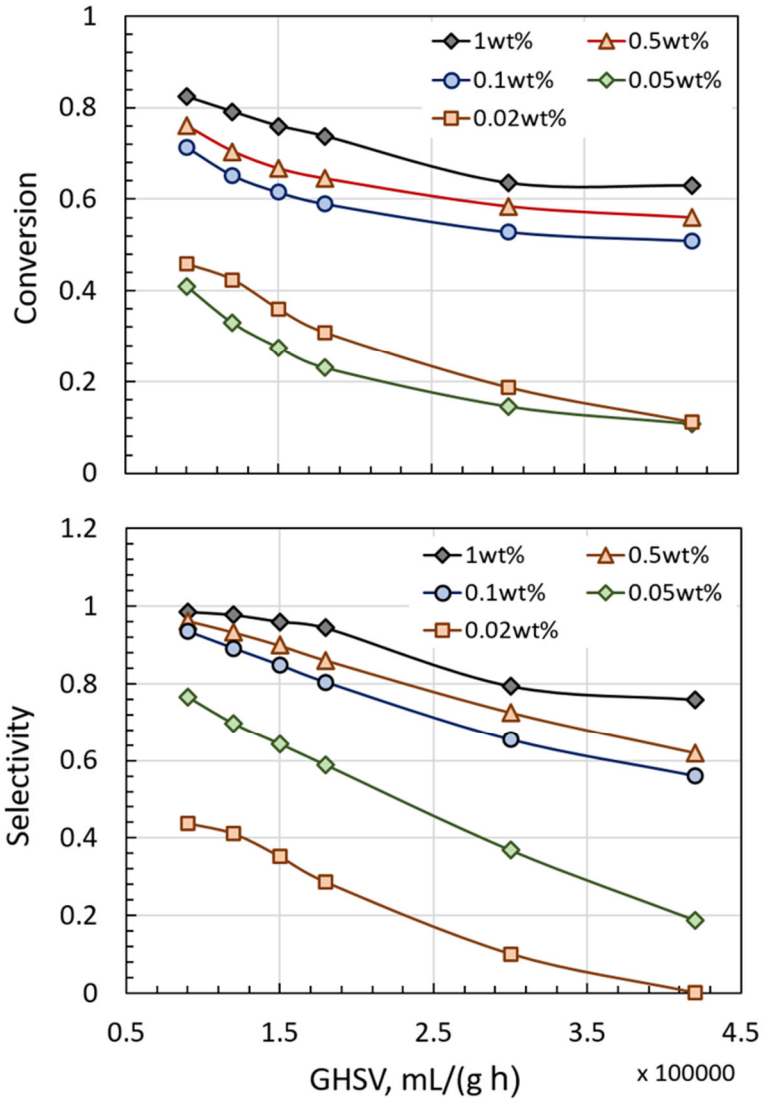

Fig. 8. CO_2 conversion and CH_4 selectivity of the 0.02-1wt% Ru/γ-Al_2O_3 catalysts as a function of space velocity. *Parameters:* T = 450 °C, H_2:CO_2 = 4, CH_4:CO_2 = 1, P = 3 bar.

The rate of CH_4 formation calculated by Eq. (10) as a function of residence time ($1/\tau$ = GHSV×ρ_b/ε, ρ_b/ε = 4 g/mL) is shown in Fig. 9a for different Ru loadings (these data correspond to Fig. 8). For the 0.1-1 wt% Ru loading catalysts, the CH_4 generation rate gradually decreases with residence time (increases with space velocity). This observation implies that the observed

decline in the CH_4 selectivity vs. GHSV (Fig. 8) should be attributed to the steeper dependence of the CO formation rate on GHSV. Namely, although the rate of CH_4 formation increases for higher GHSV, the rate of CO formation increases vs. GHSV with a higher slope. For the 0.02-0.05 wt% Ru loadings, the dependence of the CH_4 formation rate on residence time appears as completely different, with an initial sharp increase followed by a plateau for higher residence times (Fig. 9a). This observation implies that CH_4 generation will drop sharply for higher space velocities, with an opposite trend for CO formation, resulting in high selectivity to CO formation, while maintaining CO_2 conversion of 10-20% (Fig. 8).

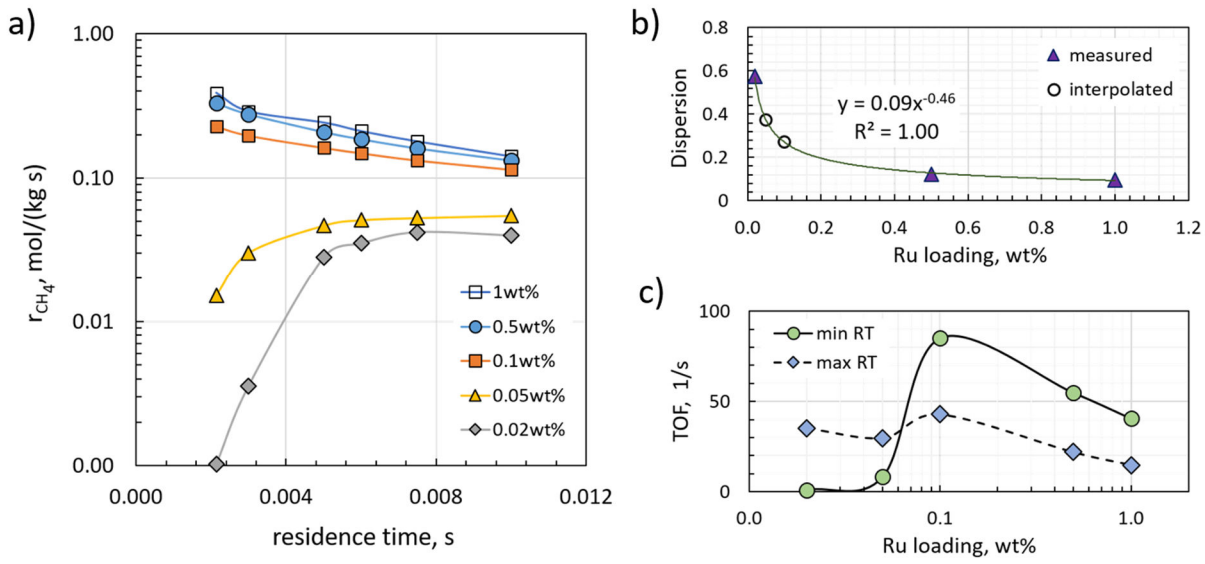

Fig. 9. CH_4 generation rate as a function of residence time for different Ru loadings (a) and the dependence of metal dispersion (b) and turnover frequency (c) on Ru loading; min RT and max RT in (c) refer to minimal/maximal residence time in (a). Parameters for (a) are as in Fig. 8.

Corresponding turnover frequencies calculated by Eq. (12) for residence times of 2×10^{-3} s (min RT) and 1×10^{-2} s (max RT) are shown in Fig. 9c. Active phase dispersion calculated from H_2 uptake (Eq. 13) is shown in Fig. 9b. The measured H_2 uptake values (Fig. 4) were fitted with a

power law equation (Fig. 9b), interpolating dispersion values for the 0.05 and 0.1 wt% Ru loadings. The TOF maximum was observed at 0.1 wt% Ru (43-85 s^{-1}). For increasing Ru loadings TOF values gradually decrease to 15-40 s^{-1} for 1 wt% Ru, while for lower Ru loading the TOF for CH_4 generation drops sharply. In view of this observation and the previously discussed conversion and selectivity trends (Figs 7, 8), decreasing Ru loading below 0.1 wt% Ru is not practical.

3.4 Stability

Catalyst stability is an important aspect of catalytic performance often overlooked in laboratory studies. There are three major pathways for catalyst deactivation, namely poisoning, sintering, and coking [3]. Since the experiments reported herein were conducted with a synthetic mixture not containing any impurities, poisoning is not expected to occur. Sintering is relevant as a deactivation mechanism, as it is induced by temperature. However, CO_2 methanation does not require high temperatures and sintering is not expected to occur to a very significant extent at 450 °C, which was the optimal temperature in terms of conversion and selectivity (Fig. 5). Coking on the other hand may occur under the methanation reaction conditions [7].

Stability tests for 0.5 wt% and 0.05 wt% Ru/γ-Al_2O_3 catalysts are shown in Fig. 10. For both catalysts, no notable deactivation was detected after 60-70 h on stream. For the 0.5 wt% Ru catalyst the conversion remained practically constant (nearly 80%) throughout the entire experiment, with the very stable selectivity to CH_4 generation of 98%. For the 0.05 wt% Ru catalyst a small decline in both conversion (from 58% to 54%) and selectivity (80% to 78%) was observed. Since the stability experiments were conducted at high space velocity (90,000 mL/(g h)) over 65-75 h on stream, it can be concluded that both catalysts did not undergo any significant deactivation.

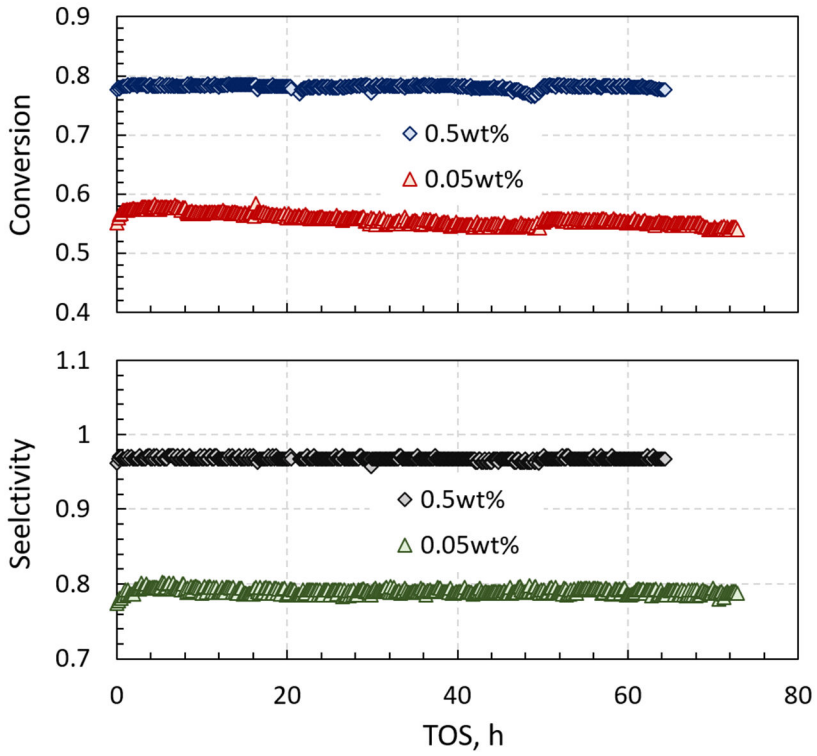

Fig. 10. Stability tests for 0.5 wt% and 0.05 wt% Ru/γ-Al_2O_3 catalysts with 50% CO_2, 50% CH_4 mixture as a feed. CO_2 conversion (upper panel) and selectivity to CH_4 formation (lower panel) are shown versus time on stream (TOS). Parameters: P = 3 bar, T = 450 °C, GHSV = 90,000 mL/(g h), H_2:CO_2 = 4.

Although no significant deactivation was observed in the stability tests, carbon deposition may still have occurred to a certain extent. To investigate the possibility and extent of coking, a temperature programed oxidation study of the 0.5 wt% Ru catalyst was conducted by TGA-FTIR, Fig. 11. The initial weight loss of 4.5% until 200 °C is attributed to physically adsorbed water and CO_2, as can be seen from H_2O and CO_2 peaks centered at 150-160 °C. An additional 2.5% weight loss occurs gradually in the 200-700 °C range. Broad peaks of CO and CO_2 are detectable in the 200-500 °C temperature range with an additional broad shoulder appearing at 600 °C. Therefore,

the 2.5% weight loss should be attributed to the removal of two types of deposited carbon that may accumulate over long periods (hundreds and thousands of hours) of operation affecting the reactor performance. On the other hand, given the high space velocity and relatively long time used in the stability tests, it can be concluded that coking was not very significant.

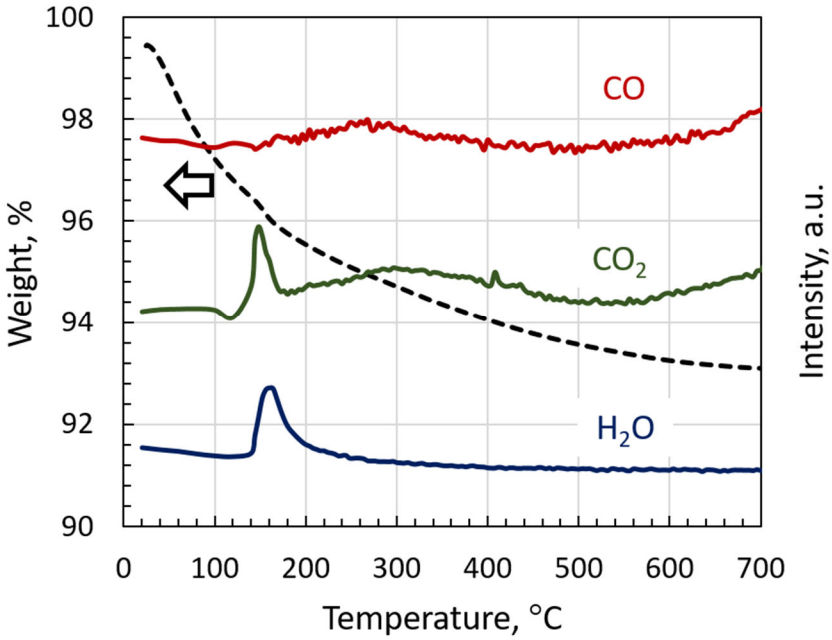

Fig. 11. Temperature programed oxidation analysis of the spent 0.5 wt% Ru/γ-Al_2O_3 catalyst after 70 h on stream under operating conditions listed in Fig. 10. The TGA curve is shown as dashed line. The FTIR signals for CO, CO_2 and H_2O were detected in the TGA exhaust line.

An additional stability test was conducted for the 0.5 wt% Ru/γ-Al_2O_3 catalyst using a more realistic feed mixture, Fig. 12. In addition to CH_4 and CO_2 as main components, biogas may also contain significant amounts of N_2, which is in particular true for landfill gas. The stability test presented in Fig. 12 was conducted with the 30% CO_2, 43% CH_4 and 27% N_2 feed mixture simulating a real landfill gas composition (after removal of impurities and water) [9]. Space

velocity was kept at a relatively low (still industrially relevant) value in order to examine the achievable upper limit of conversion.

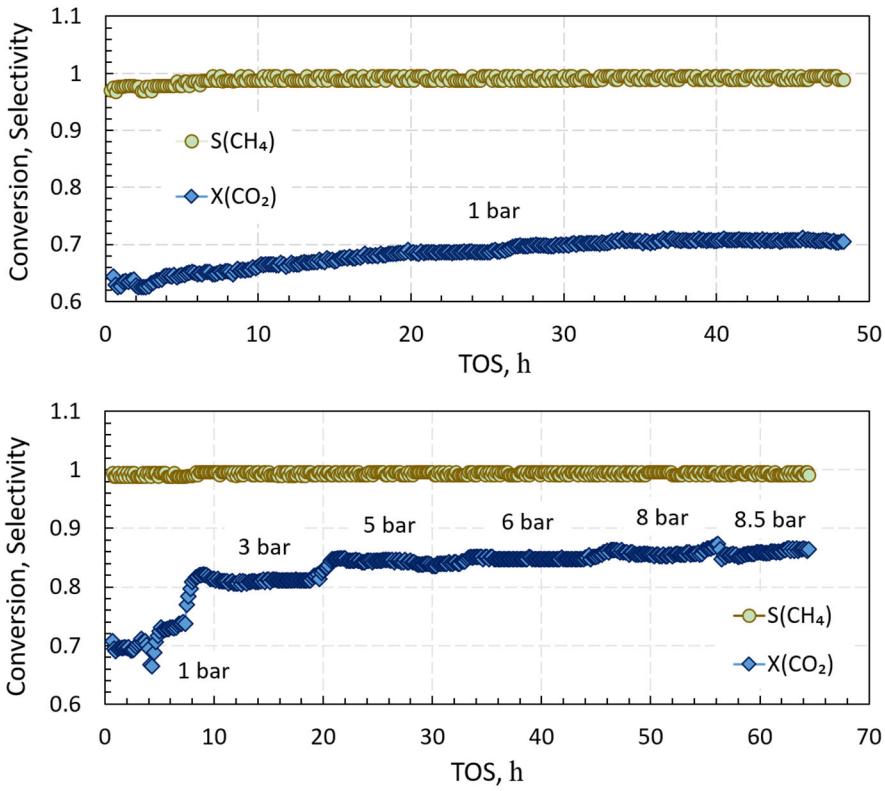

Fig. 12. Stability test of the 0.5 wt% Ru/γ-Al_2O_3 catalyst using the simulated biogas mixture containing 30% CO_2, 43% CH_4 and 27% N_2 as a feed. The lower panel shows the performance of the same catalyst (tested first at 1 bar, upper panel). Parameters: P=1-8.5 bar, T = 450 °C, GHSV = 3,000 mL/(g h), H_2:CO_2 = 4.

During the operation at 1 bar (upper panel in Fig. 12), a nearly complete selectivity to CH_4 production (99-100%) was obtained after 5 h and remained very stable until the end of test at 48 h. The CO_2 conversion gradually increased from 62% to 70% during the first 20 h of operation and remained very stable as well. As a next step, the operating pressure was gradually increase

over the additional 65 h on stream (lower panel in Fig. 12) for the same spent catalyst already used for the test shown in the upper panel of Fig. 12.

Increasing the operating pressure from 1 to 3 bar resulted in a very significant conversion gain (from 70% to 80%). Further pressure increase to 5 bar gave in an additional 5% gain in conversion. Elevating the pressure beyond this point result in a relatively minor gain in conversion. The selectivity to CH_4 generation remained complete over the course of the entire test (65 h, after initially testing the same catalyst for 48 h at 1 bar). The highest conversion was 86%, which is an excellent performance given the fact that the CO_2 content in the feed was only 30%. For 86% conversion during the operation at 8-8.5 bar the reactor outlet contained 58.1% CH_4, 15.1% H_2, 3.8% CO_2 and 23% N_2 significantly improving the quality of the gas mixture (as compared to feed composition). In practical applications N_2 will have to be removed of course (e.g., by a pressure swing adsorption (PSA) system). The unreacted H_2 on the other hand may be tolerated in certain cases such as industrial heating and a relatively small content of remaining CO_2 can be tolerated as well. Note that, assuming complete N_2 removal, the resulted composition will be 75.5% CH_4, 19.6% H_2 and 4.9% CO_2. If an additional PSA stage is applied to remove H_2, the final composition will be 93.9% CH_4 and 6.1% CO_2.

4. Conclusions

In this study the feasibility of direct conversion of CH_4-CO_2 mixtures (without CO_2 pre-separation) by Sabatier reaction using low loading Ru/γ-Al_2O_3 was investigated, to access the feasibility of direct upgrading of biogas and landfill gas into renewable natural gas (RNG). The range of Ru loadings of 0.02-1 wt% was tested using a 50:50 mixture of CO_2 and CH_4 (simulating a pre-treated biogas after removal of water and impurities). Through the catalytic performance

evaluation conducted in a range of temperatures and space velocities, it was confirmed that it is possible to achieve 80% CO_2 conversion with 99% selectivity to CH_4 formation. These values (obtained at 3 bar, 450 °C and $H_2/CO_2 = 4$ in the feed) correspond to the CO_2 conversion and CH_4 selectivity predicted by the thermodynamic equilibrium.

With the optimal operating temperature identified as 450 °C, it was also found that space velocities should be kept below 100,000 mL/(g h). Higher temperatures and space velocities result in declining CH_4 selectivity due to CO formation via the RWGS reaction, which is favored by thermodynamic equilibrium and kinetics at elevated temperatures and space velocities, respectively. These findings point out at the importance of thermal management of Sabatier reactors for which proper cooling systems have to be integrated. The upper space velocity limit of 100,000 mL/(g h) (residence time of 10 ms) does not represent any challenge because industrial processes can be conducted at much lower space velocities.

In terms of the active phase loading, the 0.1-0.5 wt% Ru content was identified as an optimal range as these loadings provide high CO_2 conversions (up to 85%) and 100% CH_4 selectivity, allowing at the same time for a significant cost reduction. Below 0.1 wt% Ru, both intrinsic activity (turnover frequency) and selectivity drop sharply, which can be attributed to the high degree of dispersion of the Ru phase that become more easily oxidized and more active in CO formation. Stability tests conducted for the 0.5 wt% Ru/γ-Al_2O_3 catalyst at 450 °C have shown that this catalysts has stable performance in terms of both conversion and selectivity over 100 h on stream, with a minor carbon deposition on the catalyst surface. The stability test conducted with the 30% CO_2, 43% CH_4 and 27% N_2 feed mixture representing a composition of landfill gas demonstrated a very stable performance as well, with 86% CO_2 conversion and 100% CH_4 selectivity.

From a practical point of view, the results presented herein indicate that it is possible to convert landfill gas or biogas to an upgraded, CH_4-enriched mixture without any CO_2 pre-separation. Removing the upstream separation step from the RNG generation system can result in a significant reduction of both capital and operating costs. Considering the abovementioned case with the 30% CO_2, 43% CH_4 and 27% N_2 feed mixture and 86% CO_2 conversion (and 100% CH_4 selectivity), the product stream composition after separating N_2 and H_2 (can be done by a PSA system) will be 93.9% CH_4 and 6.1% CO_2 (slightly higher in reality because of incomplete separation). Typical CH_4 concentration in fossil natural gas are ranging from 87-96 vol% [26]. The separated H_2 can (and should) be recycled decreasing the power consumption for water electrolysis.

Future work should include evaluation of the catalytic performance with more realistic compositions similar to those of landfill gas and biogas, and, ultimately, tests with real samples collected at landfill gas and biogas facilities. One of the issues to be addressed is catalyst stability against H_2S poisoning which will determine the acceptable H_2S levels and, thus, the extent of upstream pretreatment. The extent of coking should be also investigated over extended periods of time. Altogether, these future investigations should allow for determination of the feasibility and possible scale of the 0.5 wt% Ru/γ-Al_2O_3 catalyst application for RNG generation.

Acknowledgements

The authors acknowledge funding support from the Natural Science and Engineering Research Council (NSERC) of Canada through the Discovery Grant (RGPIN-2016-03872) and Research Tools & Instruments program (RTI-2017-00119) and from the Canada Foundation for Innovation (CFI) through the John R. Evans Leaders Fund (JELF) program (project # 35772).

Nomenclature

CB	carbon balance
d_p	particle size, nm
D	active phase dispersion
f_1	CO_2 conversion to CO
f_2	CO_2 conversion to CH_4
$F_{C,out}$	total outlet molar flow rate of carbon-containing species, mol/min
$F_{H_2,f}$	feed molar flow rate of H_2, mol/min
$F_{CO_2,f}$	feed molar flow rate of CO_2, mol/min
$F_{CO,out}$	outlet molar flow rate of CO, mol/min
$F_{CH_4,gen}$	molar flow rate of generated CH_4, mol/min
$F_{CH_4,out}$	outlet molar flow rate of CH_4, mol/min
$F_{t,out}$	total outlet molar flow rate, mol/min
$GHSV$	gas hourly space velocity, mL/(g h)
HU	chemisorption H_2 uptake, mol/g
L_{Ru}	Ru metal loading, %
M_{Ru}	atomic mass, kg/mol
r_{CH_4}	CH_4 generation rate per catalyst weight, mol/(kg s)
R_{CH_4}	CH_4 generation rate per active phase weight, mol/(kg_{Ru} s)
S_{CH_4}	selectivity to CH_4 generation
TOF	turnover frequency, 1/s
W_c	catalyst weight, kg
X_{CO_2}	CO_2 conversion
y_i	mole fraction of species i

Greek letters

α	H_2/CO_2 feed ratio

τ	residence time, s
ε	catalyst bed void fraction
β	CH_4-to-total carbon feed ratio
γ	CH_4/CO_2 feed ratio
ρ_b	catalyst bulk density, g/mL
ρ_{Ru}	Ru density, kg/m^3
ρ_{site}	active site density, $1/m^2$

References:

[1] H.-C. Shin, J.-W. Park, H.-S. Kim, E.-S. Shin, Environmental and economic assessment of landfill gas electricity generation in Korea using LEAP model, Energy Policy 33 (2005) 1261–1270.

[2] M.J. Tuinier, M. van Sint Annaland, Biogas purification using cryogenic packed bed technology, Ind. Eng. Chem. Res. 51 (2012) 5552-5558.

[3] D.S.A. Simakov, Renewable Synthetic Fuels and Chemicals from Carbon Dioxide, Springer International Publishing 2017.

[4] D. Andriani, A. Wresta, T.D. Atmaja, A. Saepudin, A review on optimization production and upgrading biogas through CO_2 removal using various techniques, Appl. Biochem. Biotechnol. 172 (2014) 1909-1928.

[5] N. Abatzoglou, S. Boivin, A review of biogas purification processes, Biofuels Bioprod. Bioref. 3 (2009) 42-71.

[6] F. Osorio, J.C. Torres, Biogas purification from anaerobic digestion in a wastewater treatment plant for biofuel production, Renew. Energy 34 (2009) 2164-2171.

[7] D. Sun, F.M. Khan, D.S.A. Simakov, Heat removal and catalyst deactivation in a Sabatier reactor for chemical fixation of CO_2: Simulation-based analysis, Chem. Eng. J. 329 (2017) 165-177.

[8] D. Sun, D.S.A. Simakov, Thermal management of a Sabatier reactor for CO_2 conversion into CH_4: Simulation-based analysis, J. CO_2 Util. 21 (2017) 368–382.

[9] R. Currie, S. Mottaghi-Tabar, Y. Zhuang, D.S.A. Simakov, Design of an air-cooled Sabatier reactor for thermocatalytic hydrogenation of CO_2: Experimental proof-of-concept and model-based feasibility analysis, Ind. Eng. Chem. Res. 58 (2019) 12964-12980.

[10] G.A. Mills, F.W. Steffgen, Catalytic methanation, Catal. Rev. 8 (1974) 159-210.

[11] G. Garbarino, D. Bellotti, P. Riani, L. Magistri, G. Busca, Methanation of carbon dioxide on Ru/Al_2O_3 and Ni/Al_2O_3 catalysts at atmospheric pressure: Catalysts activation, behaviour and stability, Int. J. Hydrog. Energy 40 (2015) 9171-9182.

[12] M.H. Amin, K. Mantri, J. Newnham, J. Tardio, S.K. Bhargava, Highly stable ytterbium promoted Ni/γ-Al_2O_3 catalysts for carbon dioxide reforming of methane, Appl. Catal. B: Environ. 119 (2012) 217-226.

[13] H. Muroyama, Y. Tsuda, T. Asakoshi, H. Masitah, T. Okanishi, T. Matsui, K. Eguchi, Carbon dioxide methanation over Ni catalysts supported on various metal oxides, J. Catal. 343 (2016) 178-184.

[14] G.D. Weatherbee, C.H. Bartholomew, Hydrogenation of CO_2 on group VIII metals: IV. Specific activities and selectivities of silica-supported Co, Fe, and Ru, J. Catal. 87 (1984) 352-362.

[15] N. Takezawa, H. Terunuma, M. Shimokawabe, H. Kobayashi, Methanation of carbon dioxide: Preparation of Ni/MgO catalysts and their performance, Appl. Catal. 23 (1986) 291-298.

[16] I.H. Son, S.J. Lee, I.Y. Song, W.S. Jeon, I. Jung, D.J. Yun, D.-W. Jeong, J.-O. Shim, W.-J. Jang, H.-S. Roh, Study on coke formation over Ni/γ-Al_2O_3, Co-Ni/γ-Al_2O_3, and Mg-Co-Ni/γ-Al_2O_3 catalysts for carbon dioxide reforming of methane, Fuel 136 (2014) 194-200.

[17] M.A. Vannice, The catalytic synthesis of hydrocarbons from carbon monoxide and hydrogen, Catal. Rev. Sci. Eng. 14 (1976) 153-191.

[18] J.H. Kwak, L. Kovarik, J. Szanyi, CO_2 reduction on supported Ru/Al_2O_3 catalysts: cluster size dependence of product selectivity, ACS Catal. 3 (2013) 2449-2455.

[19] D.S.A. Simakov, H.Y. Luo, Y. Román-Leshkov, Ultra-low loading Ru/γ-Al_2O_3: a highly active and stable catalyst for low temperature solar thermal reforming of methane, Appl. Catal. B: Environ. 168 (2015) 540-549.

[20] Z. Jiang, G. Lan, X. Liu, H. Tang, Y. Li, Solid state synthesis of Ru–MC with highly dispersed semi-embedded ruthenium nanoparticles in a porous carbon framework for benzoic acid hydrogenation, Catal. Sci. Technol. 6 (2016) 7259-7266.

[21] W. Sinkler, S.A. Bradley, U. Ziese, K.P. de Jong, 3D-TEM study of gamma alumina catalyst supports, Microsc. Microanal. 12 (2006) 52-53.

[22] Y. Liu, F.-Y. Huang, J.-M. Li, W.-Z. Weng, C.-R. Luo, M.-L. Wang, W.-S. Xia, C.-J. Huang, H.-L. Wan, In situ Raman study on the partial oxidation of methane to synthesis gas over Rh/Al_2O_3 and Ru/Al_2O_3 catalysts, J. Catal. 256 (2008) 192-203.

[23] I. Balint, A. Miyazaki, K.-i. Aika, Methane reaction with NO over alumina-supported Ru nanoparticles, J. Catal. 207 (2002) 66-75.

[24] P. Betancourt, A. Rives, R. Hubaut, C.E. Scott, J. Goldwasser, A study of the ruthenium–alumina system, Appl. Catal A: Gen. 170 (1998) 307-314.

[25] H. Madhavaram, H. Idriss, S. Wendt, Y.D. Kim, M. Knapp, H. Over, J. Aßmann, E. Löffler, M. Muhler, Oxidation reactions over RuO_2: a comparative study of the reactivity of the (110) single crystal and polycrystalline surfaces, J. Catal. 202 (2001) 296-307.

[26] A. Demirbas, Methane Gas Hydrate: as a Natural Gas Source. In: Methane Gas Hydrate. Green Energy and Technology, Springer, London, 2010.

[27] K. Hou, R. Hughes, The kinetics of methane steam reforming over a Ni/a-Al_2O_3 catalyst, Chem. Eng. J. 82 (2001) 311-328.

Appendix

Sabatier reaction-reverse water gas shift (RWGS) equilibrium calculation

Assuming no carbon deposition, the equilibrium conversion and selectivity can be calculated using the Sabatier reaction-RWGS system shown below:

$$CO_2 + H_2 \rightleftarrows CO + H_2O \qquad \Delta H^{\circ}_{298} = 41 \text{ kJ/mol} \tag{A1}$$

$$CO_2 + 4H_2 \rightleftarrows CH_4 + 2H_2O \qquad \Delta H^{\circ}_{298} = -164.9 \text{ kJ/mol} \tag{A2}$$

First, equilibrium constants for the RWGS and Sabatier reaction are written in terms of partial pressures:

$$K_{eq,1} = \frac{p_{CO} p_{H_2O}}{p_{CO_2} p_{H_2}} \tag{A3}$$

$$K_{eq,2} = \frac{p_{CH_4} p_{H_2O}^2}{p_{CO_2} p_{H_2}^4} \tag{A4}$$

Both equilibrium constants can be also expressed as a function of temperature:

$$K_{eq,1} = A_1 \exp\left(\frac{-E_{eq,1}}{R_g T}\right) \tag{A5}$$

$$K_{eq,2} = A_2 \exp\left(\frac{-E_{eq,2}}{R_g T}\right) \tag{A6}$$

Next, CO_2 conversion to CO and CH_4 are defined as follows:

$$f_1 = \frac{n_{CO,eq}}{n_{CO_2,f}} \tag{A7}$$

$$f_2 = \frac{n_{CH_4,eq}}{n_{CO_2,f}} \tag{A8}$$

The extents of all species in the thermodynamic equilibrium can be now expressed as a function of f_1 and f_2:

$$\begin{aligned} \phi_{CO_2} &= 1 - f_1 - f_2 \\ \phi_{H_2} &= \alpha - f_1 - 4f_2 \\ \phi_{CO} &= f_1 \\ \phi_{CH_4} &= \gamma + f_2 \\ \phi_{H_2O} &= f_1 + 2f_2 \end{aligned} \tag{A9}$$

The feed composition parameters α and γ are defined as the H_2:CO_2 and CH_4:CO_2 feed ratios:

$$\begin{aligned} \alpha &= \frac{n_{H_2,f}}{n_{CO_2,f}} \\ \gamma &= \frac{n_{CH_4,f}}{n_{CO_2,f}} \end{aligned} \tag{A10}$$

Equilibrium partial pressures can written in terms of species extent (y_i is mole fraction and P is the total pressure of the reaction system):

$$p_i = y_i P = \frac{\phi_i}{\sum \phi_i} P \tag{A11}$$

Combining Eqs (A3-6) and expending using Eqs (A9-11):

$$\frac{f_1(f_1+2f_2)}{(1-f_1-f_2)(\alpha-f_1-4f_2)} = A_1 \exp\left(\frac{-E_{eq,1}}{R_g T}\right) \tag{A12}$$

$$\frac{(\gamma+f_2)(f_1+2f_2)^2(1+\alpha+\gamma-2f_2)^2}{(1-f_1-f_2)(\alpha-f_1-4f_2)^4} = P^2 A_2 \exp\left(\frac{-E_{eq,2}}{R_g T}\right) \tag{A13}$$

Eqs (A12, A13) are solved numerically to obtain f_1 and f_2 as a function of T for the given feed composition (α, γ) and pressure (P). Finally, the equilibrium conversion and selectivity are calculated using Eqs (4a) and (5a). Thermodynamic parameters A_1, A_2, $E_{eq,1}$ and $E_{eq,2}$ can be found in the literature [27].